IEEE Access
Multidisciplinary | Rapid Review | Open Access Journal

Received February 20, 2020, accepted March 2, 2020, date of publication March 11, 2020, date of current version March 20, 2020.

Digital Object Identifier 10.1109/ACCESS.2020.2979995

Distributed Event-Triggered Adaptive Formation Tracking of Networked Uncertain Stratospheric Airships Using Neural Networks

JIN HOE KIM AND SUNG JIN YOO

School of Electrical and Electronics Engineering, Chung-Ang University, Seoul 06974, South Korea

Corresponding author: Sung Jin Yoo (sjyoo@cau.ac.kr)

This work was supported in part by the Chung-Ang University Graduate Research Scholarship in 2019, in part by the Human Resources Development of the Korea Institute of Energy Technology Evaluation and Planning (KETEP) funded by the Korea Government Ministry of Trade, Industry and Energy under Grant 20174030201810, and in part by the National Research Foundation of Korea (NRF) funded by the Korea Government under Grant NRF-2019R1A2C1004898.

ABSTRACT This paper investigates a distributed event-triggered formation tracking problem of networked three-dimensional uncertain nonlinear stratospheric airships under directed networks. It is assumed that the nonlinearities of airship followers are unknown and the leader information can be obtained by only a subset of the airship followers. Approximation-based local adaptive tracking controllers with asynchronous event-triggering laws are developed to achieve the desired formations for both the positions and attitudes of uncertain stratospheric airship followers. We theoretically show that the stability and formation tracking performance of event-triggered closed-loop systems are ensured and Zeno behavior is excluded in the proposed asynchronous event-triggering mechanism. Finally, simulations illustrate the effectiveness of the proposed formation control protocol.

INDEX TERMS Distributed adaptive formation tracking, event-triggered, neural networks, networked stratospheric airships.

I. INTRODUCTION

Because of various advantages such as high-altitude scientific explorations, vertical landing and takeoff, long time keeping in space, and better communications and real-time surveillance than satellites [1]–[4], stratospheric airships have received increasing attention from control designers. The initial studies focused on the stabilization problem of stratospheric airships. In [5], a linearized model of airships was presented and its linear control strategy was derived. Nonlinear control design approaches such as sliding mode control [6] and dynamic inversion control [7] have been studied for nonlinear stratospheric airships. For more practical applications, the tracking problem has actively been addressed for nonlinear stratospheric airships. In [8], the guidance-based path-following principle was employed to design a three-dimensional path-following controller for nonlinear airships. By augmenting a fixed-time control design with power integrators, a fixed-time trajectory tracking control problem of stratospheric airships was addressed in [9]. For airship models subject to unknown system parameters, a nonlinear trajectory tracking control approach was studied in [10] where the unknown parameters were compensated by an adaptive mechanism. Adaptive approximation techniques [11]–[13] have been employed to estimate unknown nonlinearities of airships in adaptive backstepping and sliding mode control frameworks [14], [15]. Despite these efforts, the existing tracking control strategies [8]–[10], [14], [15] for nonlinear airship models have the following restrictions.

(R1) The existing methods [8]–[10], [14], [15] can only be applied to the tracking control problem of single nonlinear stratospheric airships. The distributed formation control problem of networked multiple nonlinear stratospheric airships is still open in the control field of stratospheric airships. This problem is particularly challenging because the positions and attitudes of multiple nonlinear stratospheric airships in a three-dimensional space need to be simultaneously considered to design a formation tracking scheme under the limitation of communication links.

The associate editor coordinating the review of this manuscript and approving it for publication was Shuping He.

(R2) The existing methods [8]–[10], [14], [15] cannot be applied to the networked control problem of nonlinear stratospheric airships with limited network resources because the tracking control laws are continuously updated. For a more practical control problem, an event-triggered formation control strategy needs to be developed for networked multiple nonlinear stratospheric airships.

Event-triggered control has been a subject of interest to the control community because of the efficient management of control signals in limited network resources [16], [17]. In [23] and [24], control problems in the presence of signal quantization were addressed for uncertain linear systems. In [18]–[22], event-triggered control schemes have been proposed for linear and nonlinear systems. For uncertain nonlinear systems, adaptive function-approximation-based event-triggered control designs were studied in [25]–[27]. Based on these theoretical foundations, event-triggered control results have been extended to practical applications such as quadrotors [28], mobile robots [29], and flexible-link manipulators [30]. However, no research results are available yet on the event-triggered control problem of uncertain nonlinear stratospheric airships. Thus, a distributed event-triggered formation tracking issue of positions and attitudes of networked airships also exists.

Motivated by these observations, we propose a distributed event-triggered formation tracking control strategy for uncertain multiple three-dimensional nonlinear stratospheric airships under directed communication networks. The local event-triggered tracking laws and their asynchronous triggering laws are designed for the formation control of both the positions and attitudes of airships in the distributed dynamic surface design framework. In the local control laws, radial basis function neural networks are employed as function approximators in order to compensate for unknown nonlinearities of the airship's dynamics. The stability of the resulting closed-loop system and the existence of the minimum inter-event times are rigorously analyzed in the sense of Lyapunov and simulation results are presented to demonstrate the effectiveness of the proposed control strategy.

The main contributions of this paper are emphasized as follows.

(C1) In contrast to the existing control results for single stratospheric airships [5]–[10], we firstly investigate the distributed formation control problem of networked multiple stratospheric airships with heterogeneous unknown nonlinearities. In addition, both the positions and attitudes of airships in a three-dimensional space are considered for the formation control problem.

(C2) An asynchronous event-triggered formation control problem is firstly addressed for networked multiple stratospheric airships. The proposed control law for each airship is updated intermittently by deriving the triggering law to avoid the unnecessary updating of control signals reported in [5]–[10].

The rest of this paper is organized as follows. In Section II-A, we introduce the kinematics and dynamics of the networked stratospheric airships. The distributed event-triggered formation tracking problem of multiple airships is formulated in Section II-B. Then, a distributed event-triggered multi-airship formation tracking scheme is designed in Section III-A and the closed-loop stability is rigorously analyzed in Section III-B. In Section IV, simulation results are given. Finally, conclusions are provided in Section V.

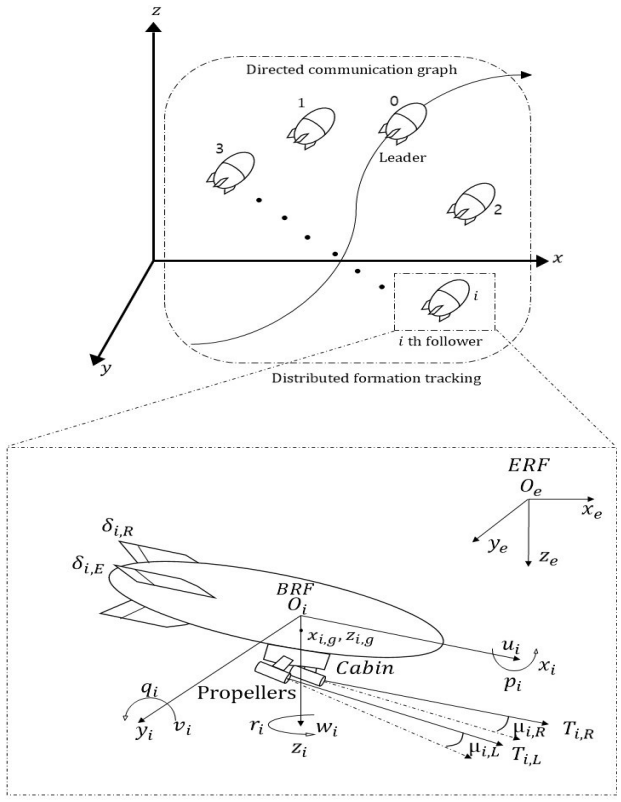

FIGURE 1. The *i*th airship.

II. PROBLEM FORMULATION

A. KINEMATICS AND DYNAMICS OF NETWORKED MULTIPLE STRATOSPHERIC AIRSHIPS

In this study, we consider networked stratospheric airship models composed of N followers, labeled as $1, \ldots, N$, and a leader, labeled as 0, under a directed communication topology. The structure of the networked multiple unmanned stratospheric airships is shown in Fig. 1. Each airship has a traditional ellipsoidal shape and a symmetric cabin with respect to the longitudinal axis. Two propellers for generating thrust are fixed at each side of the cabin. Two rudders and two elevators installed at the empennage of the airship are used to control the yaw and pitch movements, respectively. For each airship model, there are an earth reference frame (ERF) and a body reference frame (BRF). The ERF is represented by x_e, y_e, and z_e axes, and its origin is denoted as O_e. The $O_e x_e$ and $O_e z_e$ axes point toward the north and core of the earth, respectively, and the $O_e y_e$ direction is determined using

the right-hand rule. The BRF of the ith airship is described by x_i, y_i, and z_i axes, and its origin is defined as the center O_i of the ith airship's volume. The O_ix_i and O_iz_i axes point toward the head and downward of the ith airship, respectively, and the direction of O_iy_i is found using the right-hand rule.

The limited network communication of the N airship followers and a leader is described by a directed graph $\mathcal{G} \triangleq (\mathcal{V}, \mathcal{E})$ where $\mathcal{V} \triangleq \{0, 1, \ldots, N\}$ and $\mathcal{E} \subseteq \mathcal{V} \times \mathcal{V}$ are the sets of nodes and edges, respectively. An edge (j, i) implies that the information of agent j can be transmitted to agent i, but not vice versa. $\mathcal{N}_i = \{j | (j, i) \in \mathcal{E}\}$ means the neighbors' set of node i where $i = 1, \ldots, N, j = 0, \ldots, N$, and $i \neq j$. For the communication of N airship followers, the subgraph $\bar{\mathcal{G}} \triangleq (\bar{\mathcal{V}}, \bar{\mathcal{E}})$ is defined where $\bar{\mathcal{V}} \triangleq \{1, \ldots, N\}$ and $\bar{\mathcal{E}} \subseteq \bar{\mathcal{V}} \times \bar{\mathcal{V}}$ are the sets of nodes and edges, respectively. The adjacent matrix $\mathcal{H}$ for $\bar{\mathcal{G}}$ is defined as $\mathcal{H} = [h_{i,j}] \in \mathbb{R}^{N\times N}$ where $h_{i,j} > 0$ if $(j, i) \in \mathcal{E}$ and $h_{i,j} = 0$ otherwise, and $h_{i,i} = 0$. The in-degree b_i of node i is defined as $b_i = \sum_{j=1, j\neq i}^{N} h_{i,j}$. A diagonal matrix $\mathcal{B} = \text{diag}[b_1, \ldots, b_N]$ is called the degree matrix. The Laplacian matrix $\mathcal{L}$ for $\mathcal{G}$ is $\mathcal{L} = \begin{bmatrix} 0 & 0_{1\times N} \\ -s & \bar{\mathcal{L}} + \mathcal{S} \end{bmatrix}$ and nonsymmetric where $s = [s_1, \ldots, s_N]^\top$, $\bar{\mathcal{L}} = \mathcal{B} - \mathcal{H} \in \mathbb{R}^{N\times N}$, and $\mathcal{S} = \text{diag}[s_1, \ldots, s_N]$. Here, $s_i > 0$ if the leader $0 \in \mathcal{N}_i$, and $s_i = 0$ otherwise.

The model of the follower is selected based on [10]. The kinematic equations of the ith airship are given by

$$\dot{\eta}_i = R_{i,1}(\zeta_i)\upsilon_i, \quad \dot{\zeta}_i = R_{i,2}(\zeta_i)\omega_i \tag{1}$$

where $i = 1, \ldots, N$, $\eta_i = [x_i, y_i, z_i]^\top$ are the inertial positions of the center O_i of the ith airship and $\zeta_i = [\phi_i, \theta_i, \psi_i]^\top$ are the attitude of the ith airship described by the Euler angles in the ERF; $\upsilon_i = [u_i, v_i, w_i]^\top$ and $\omega_i = [p_i, q_i, r_i]^\top$ denote the translational and rotational velocities of the ith airship defined in the BRF, respectively, $R_{i,1}(\zeta_i)$ and $R_{i,2}(\zeta_i)$ are defined as

$$R_{i,1}(\zeta_i) = \begin{bmatrix} c_{\theta_i}c_{\psi_i} & s_{\theta_i}c_{\psi_i}s_{\phi_i} - s_{\psi_i}c_{\phi_i} & s_{\theta_i}c_{\psi_i}c_{\phi_i} + s_{\psi_i}s_{\phi_i} \\ c_{\theta_i}s_{\psi_i} & s_{\theta_i}s_{\psi_i}s_{\phi_i} + c_{\psi_i}c_{\phi_i} & s_{\theta_i}s_{\psi_i}c_{\phi_i} - c_{\psi_i}s_{\phi_i} \\ -s_{\theta_i} & c_{\theta_i}s_{\phi_i} & c_{\theta_i}c_{\phi_i} \end{bmatrix},$$

$$R_{i,2}(\zeta_i) = \begin{bmatrix} 1 & t_{\theta_i}s_{\phi_i} & t_{\theta_i}c_{\phi_i} \\ 0 & c_{\phi_i} & -s_{\phi_i} \\ 0 & s_{\phi_i}/c_{\theta_i} & c_{\phi_i}/c_{\theta_i} \end{bmatrix}$$

where $s_{(\cdot)} \triangleq \sin(\cdot)$, $c_{(\cdot)} \triangleq \cos(\cdot)$, and $t_{(\cdot)} \triangleq \tan(\cdot)$. The kinematics (1) can be rewritten as

$$\begin{bmatrix} \dot{\eta}_i \\ \dot{\zeta}_i \end{bmatrix} = \begin{bmatrix} R_{i,1}(\zeta_i) & 0 \\ 0 & R_{i,2}(\zeta_i) \end{bmatrix} \begin{bmatrix} \upsilon_i \\ \omega_i \end{bmatrix}. \tag{2}$$

The dynamics of the ith airship is given by

$$M_i \begin{bmatrix} \dot{\upsilon}_i \\ \dot{\omega}_i \end{bmatrix} = N_i(\upsilon_i, \omega_i) + G_i(\zeta_i) + D_i(\upsilon_i)\tau_i \tag{3}$$

where M_i, $N_i(\upsilon_i, \omega_i)$, $G_i(\zeta_i)$, and $D_i(\upsilon_i)$ are defined at the bottom of this page, $\tau_i \triangleq [T_{i,R}s_{\mu_{i,R}}, \delta_{i,R}, \delta_{i,E}, T_{i,L}c_{\mu_{i,L}}, T_{i,R}c_{\mu_{i,R}}, T_{i,L}s_{\mu_{i,L}}]^\top$; $T_{i,R}$ and $T_{i,L}$ are the thrusts of the right and left propellers of the ith airship, respectively, $\mu_{i,R}$ and $\mu_{i,L}$ are the right and left rotation angles around the horizontal axis of the ith airship, respectively, and $\delta_{i,R}$ and $\delta_{i,E}$ represent the deflections of the rudders and elevators of the ith airship, respectively. The system parameters in M_i, $N_i(\upsilon_i, \omega_i)$, $G_i(\zeta_i)$, and $D_i(\upsilon_i)$ are defined as follows: m_i and Λ_i are the mass and volume of the ith airship, respectively, $x_{i,g}$ and $z_{i,g}$ are the x_i- and z_i-coordinates of the center of mass of the ith airship, respectively, $k_{i,1}$, $k_{i,2}$, and $k_{i,3}$ denote the ellipsoidal inertia factors to calculate the added mass and inertia matrices, ρ_i is the atmospheric density of the flight attitude of the ith airship, $V_i = \sqrt{(u_i - u_{i,\omega})^2 + (v_i - v_{i,\omega})^2 + (w_i - w_{i,\omega})^2}$ is the relative speed of the ith airship with wind velocities $u_{i,\omega}$, $v_{i,\omega}$, and $w_{i,\omega}$ [31], $\{I_{i,x}, I_{i,y}, I_{i,z}\}$ and $\{I_{i,xy}, I_{i,yz}, I_{i,xz}\}$ represent the moments of inertia and the products of two moments

$$M_i = \begin{bmatrix} m_i + \rho_i \bigwedge_i k_{i,1} & 0 & 0 & 0 & m_iz_{i,g} & 0 \\ 0 & m_i + \rho_i \bigwedge_i k_{i,2} & 0 & -m_iz_{i,g} & 0 & m_ix_{i,g} \\ 0 & 0 & m_i + \rho_i \bigwedge_i k_{i,2} & 0 & -m_ix_{i,g} & 0 \\ 0 & -m_iz_{i,g} & 0 & I_{i,x} & 0 & -I_{i,xz} \\ m_iz_{i,g} & 0 & -m_ix_{i,g} & 0 & I_{i,z} + \rho_i \bigwedge_i k_{i,3} & 0 \\ 0 & m_ix_{i,g} & 0 & -I_{i,xz} & 0 & I_{i,z} + \rho_i \bigwedge_i k_{i,3} \end{bmatrix},$$

$$N_i(\upsilon_i, \omega_i) = \begin{bmatrix} (m_i + \rho_i \bigwedge_i k_{i,2})(v_ir_i - w_iq_i) - m_iz_{i,g}p_ir_i - \frac{1}{2}\rho_iV_i^2(C_{i,X1}c_{\alpha_i}^2c_{\beta_i}^2 + C_{i,X2}s_{2\alpha_i}s_{\alpha_i/2}) + m_ix_{i,g}(q_i^2 + r_i^2) \\ (m_i + \rho_i \bigwedge_i k_{i,2})w_ip_i - (m_i + \rho_i \bigwedge_i k_{i,1})u_ir_i - m_iz_{i,g}q_ir_i - \frac{1}{2}\rho_iV_i^2(C_{i,Y1}c_{\beta_i/2}s_{2\beta_i} + C_{i,Y2}s_{2\beta_i} + C_{i,Y3}s_{\beta_i}s_{|\beta_i|}) - m_ix_{i,g}p_iq_i \\ (m_i + \rho_i \bigwedge_i k_{i,1})u_iq_i - (m_i + \rho_i \bigwedge_i k_{i,2})v_ip_i + m_iz_{i,g}(q_i^2 + p_i^2) - \frac{1}{2}\rho_iV_i^2(C_{i,Z1}c_{\alpha_i/2}s_{2\alpha_i} + C_{i,Z2}s_{2\alpha_i} + C_{i,Z3}s_{\alpha_i}s_{|\alpha_i|}) - m_ix_{i,g}r_ip_i \\ (I_{i,y} - I_{i,z})q_ir_i + I_{i,xz}p_iq_i + m_iz_{i,g}(u_ir_i - w_ip_i) + \frac{1}{2}\rho_iV_i^2C_{i,L1}s_{\beta_i}s_{|\beta_i|} + m_ix_g(v_ip_i - u_iq_i) \\ (\rho_i \bigwedge_i k_{i,3} + I_{i,z} - I_{i,x})p_iq_i - I_{i,xz}(p_i^2 + q_i^2) + m_iz_{i,g}(v_ir_i - w_iq_i) - \frac{1}{2}\rho_iV_i^2((C_{i,M1}c_{\alpha_i/2} + C_{i,M2})s_{2\alpha_i} + C_{i,M3}s_{\alpha_i}s_{|\alpha_i|}) - m_ix_{i,g}(u_ir_i - w_ip_i) \\ (I_{i,x} - I_{i,y} - \rho_i \bigwedge_i k_{i,3})p_iq_i - I_{i,xz}q_ir_i + \frac{1}{2}\rho_iV_i^2(C_{i,N1}c_{\beta_i/2}s_{2\beta_i} + C_{i,N2}s_{2\beta_i} + C_{i,N3}s_{\beta_i}s_{|\beta_i|}) \end{bmatrix},$$

$$G_i(\zeta_i) = \begin{bmatrix} (\Theta_i - m_ig)s_{\theta_i} \\ -(\Theta_i - m_ig)c_{\theta_i}s_{\phi_i} \\ -(\Theta_i - m_ig)c_{\theta_i}c_{\phi_i} \\ -z_{i,g}m_igc_{\theta_i}s_{\phi_i} \\ -z_{i,g}m_igs_{\theta_i} - x_{i,g}m_igc_{\theta_i}c_{\phi_i} \\ x_{i,g}m_igc_{\theta_i}s_{\phi_i} \end{bmatrix} \quad D_i(\upsilon_i) = \begin{bmatrix} -y_{i,p} & 0 & 0 & -z_{i,p}s_{\chi_i} & -z_{i,p}s_{\chi_i} & y_{i,p} \\ -x_{i,p} & 2Q_iC_{i,Y4} & 0 & z_{i,p}c_{\chi_i} & z_{i,p}c_{\chi_i} & -x_{i,p} \\ 0 & 0 & -2Q_iC_{i,Z4} & x_{i,p}s_{\chi_i} - y_{i,p}c_{\chi_i} & x_{i,p}s_{\chi_i} + y_{i,p}c_{\chi_i} & 0 \\ 0 & 0 & 0 & c_{\chi_i} & c_{\chi_i} & 0 \\ 0 & 0 & -2Q_iC_{i,M4} & s_{\chi_i} & -s_{\chi_i} & 0 \\ 1 & -2Q_iC_{i,N4} & 0 & 0 & 0 & 1 \end{bmatrix}$$

of inertia in BRF, respectively, $\alpha_i = \arctan(w_i, u_i)$, $\beta_i = \arctan(v_i \cos\alpha_i, u_i)$, Θ_i denotes the buoyancy that acts on the ith airship, g is the gravitational acceleration, $Q_i = \rho_i V_i^2/2$ denotes the dynamic pressure of the ith airship, $C_{i,X1}$, $C_{i,X2}$, $C_{i,Y1}, \ldots, C_{i,Y4}$, $C_{i,Z1}, \ldots, C_{i,Z4}$, $C_{i,L1}$, $C_{i,M1}, \ldots, C_{i,M3}$, and $C_{i,N1}, \ldots, C_{i,N4}$ denote the aerodynamic coefficients, $\{x_{i,p}, y_{i,p}, z_{i,p}\}$ are the position coordinates of the right propeller of the ith airship in the BRF, and χ_i means the patulous angle of the ith airship. We assume that the buoyant state of the airship is neutral, i.e., $m_i g = \Theta_i$ [8]. Because of the symmetric structure of the cabin, it holds that $I_{i,xy} = 0$ and $I_{i,yz} = 0$.

B. PROBLEM STATEMENT

The kinematics and dynamics of the ith airship follower are summarized by the following state-space form

$$\begin{aligned} \dot{x}_{i,1} &= P_i(x_{i,1})x_{i,2}, \\ \dot{x}_{i,2} &= M_i^{-1}(\bar{G}_i(x_{i,1}, x_{i,2}) + D_i\tau_i), \\ \varpi_i &= x_{i,1}, \end{aligned} \tag{4}$$

where $i = 1, \ldots, N$, $x_{i,1} = [\eta_i^\top, \zeta_i^\top]^\top$, $x_{i,2} = [\upsilon_i^\top, \omega_i^\top]^\top$ $\bar{G}_i = N_i(\upsilon_i, \omega_i) + G_i(\zeta_i)$, $P_i = \mathrm{diag}[R_{i,1}(\zeta_i), R_{i,2}(\zeta_i)]$, τ_i is the control input vector of the ith airship, and ϖ_i is the output vector of the ith airship. Note that the control vector τ_i is updated not continuously but intermittently in time by deriving an event-triggering mechanism to be designed later.

Problem 1: Consider networked unmanned stratospheric airships (4) under directed networks. Our control problem is to design distributed event-triggered adaptive formation tracking control laws τ_i to achieve the desired formations for both the positions and attitudes of networked uncertain stratospheric airship followers in a three-dimensional space.

Assumption 1: The system nonlinearity $\bar{G}_i$ of the dynamics in (4) is unknown where $i = 1, \ldots, N$.

Assumption 2: The leader output signal $\varpi_0 \in \mathbb{R}^6$ and its derivatives $\dot{\varpi}_0 \in \mathbb{R}^6$ and $\ddot{\varpi}_0 \in \mathbb{R}^6$ are bounded and the ith follower satisfying $0 \in \mathcal{N}_i$, $i = 1, \ldots, N$, can obtain information for ϖ_0 and $\dot{\varpi}_0$.

Assumption 3: The augmented directed graph $\mathcal{G}$ has a spanning tree with the leader as the root node.

Remark 1: In the existing tracking control results for stratospheric airships [8]–[10], [14], [15], only single airships are considered and their tracking controllers should be updated constantly. Therefore, the results [8]–[10], [14], [15] cannot provide a solution to the distributed event-triggered formation tracking problem of networked stratospheric airships formulated in Problem 1. To the best of our knowledge, our study is the first trial in the tracking control field of stratospheric airships.

Definition 1 [32]: The solutions for systems (4) are said to be semi-globally uniformly ultimately bounded if there exist adjustable constants $\Delta > 0$ and $\Psi > 0$, independent of $t_0 \geq 0$, and for every $\varphi \in (0, \Delta)$, there is $T \geq 0$, independent of t_0 such that $\|\bar{x}(t_0)\| \leq \varphi \Rightarrow \|\bar{x}(t)\| \leq \Psi$ for all $t \geq t_0 + T$, where $\bar{x} = [\bar{x}_1^\top, \ldots, \bar{x}_N^\top]^\top$; $\bar{x}_i = [x_{i,1}^\top, x_{i,2}^\top]^\top$.

III. DISTRIBUTED EVENT-TRIGGERED MULTI-AIRSHIP FORMATION TRACKING

A. DISTRIBUTED EVENT-TRIGGERED FORMATION TRACKER DESIGN

By adopting the distributed dynamic surface design concept [33], the error surfaces $z_{i,1}$ and $z_{i,2}$ and the boundary layer error c_i are defined by

$$\begin{aligned} z_{i,1} &= \sum_{j=1}^{N} h_{i,j}(\varpi_i - \varpi_j - \bar{o}_{i,j}) + s_i(\varpi_i - \varpi_0 - \bar{o}_{i,0}), \\ z_{i,2} &= x_{i,2} - \bar{\nu}_i, \\ c_i &= \bar{\nu}_i - \nu_i, \end{aligned} \tag{5}$$

where $i = 1, \ldots, N$, $\bar{o}_{i,j}$ and $\bar{o}_{i,0}$ are the offsets to make the desired formations between airships i and j and between airship i and the leader, respectively, and ν_i and $\bar{\nu}_i$ are virtual control laws and filtered virtual control laws, respectively. The filtered virtual control laws $\bar{\nu}_i$ are obtained using the following first-order low-pass filter

$$\xi_i \dot{\bar{\nu}}_i + \bar{\nu}_i = \nu_i, \quad \bar{\nu}_i(0) = \nu_i(0) \tag{6}$$

where $\xi_i > 0$ denotes a small time constant.

The design procedure comprises two steps.

Step 1: The time derivative of the first error surface $z_{i,1}$ using (5) is given by

$$\begin{aligned} \dot{z}_{i,1} &= \sum_{j=1}^{N} h_{i,j}(\dot{\varpi}_i - \dot{\varpi}_j) + s_i(\dot{\varpi}_i - \dot{\varpi}_0) \\ &= (s_i + b_i)P_i(z_{i,2} + c_i + \nu_i) - \sum_{j=1}^{K} h_{i,j}P_j x_{j,2} - s_i\dot{\varpi}_0 \end{aligned} \tag{7}$$

where $i = 1, \ldots, N$.

Then, we design the virtual control law ν_i for stabilizing (7) as follows:

$$\nu_i = \frac{1}{(s_i + b_i)} P_i^{-1}\left[-\kappa_{i,1} z_{i,1} + \sum_{j=1}^{K} h_{i,j}P_j x_{j,2} + s_i\dot{\varpi}_0 \right] \tag{8}$$

where $i = 1, \ldots, N$, $\kappa_{i,1} = \mathrm{diag}[\kappa_{i,1,1}, \ldots, \kappa_{i,1,6}]$; $\kappa_{i,1,l} > 0$, $l = 1, \ldots, 6$, are design constants. Notice that $R_{i,1}$ is non-singular and $R_{i,2}$ is also non-singular due to $|\phi_i| < \pi$ and $|\theta_i| < \pi/2$ [10]. Thus, it is ensured that P_i is invertible.

A Lyapunov function candidate is defined as $V_{i,1} = (1/2)z_{i,1}^\top z_{i,1}$ for $i = 1, \ldots, N$. By substituting (8) into (7), the time derivative of $V_{i,1}$ satisfies

$$\dot{V}_{i,1} = -z_{i,1}^\top \kappa_{i,1} z_{i,1} + (s_i + b_i)z_{i,1}^\top P_i(z_{i,2} + c_i). \tag{9}$$

Remark 2: The design of the virtual controller (8) is based on the Lyapunov stability theory [32]. A Lyapunov function $V_{i,1}$ is defined using the error surface $z_{i,1}$ and the virtual controller ν_i is chosen to induce a negative term $-z_{i,1}^\top \kappa_{i,1} z_{i,1}$ in $\dot{V}_{i,1}$ while compensating for the term $-\sum_{j=1}^{K} h_{i,j}P_j x_{j,2} - s_i\dot{\varpi}_0$ in (7) (see (9)). With the help of the negative term and the recursive design procedure, we can ensure the boundedness of $z_{i,1}$ (see the proof of Theorem 1–(i)).

Step 2: From (4) and (5), the time derivative of the second error surface $z_{i,2}$ is given by

$$\dot{z}_{i,2} = M_i^{-1}(\bar{G}_i + D_i\tau_i) - \dot{\bar{\nu}}_i. \tag{10}$$

For the online approximation of the unknown nonlinear function vector $\bar{G}_i$, radial basis function neural networks [34] are employed as function approximators. The unknown nonlinear function $\bar{G}_i$ is approximated to a sufficient degree of accuracy as follows:

$$\bar{G}_i(\bar{x}_i) = W_i^{*\top}\varphi_i(\bar{x}_i) + \epsilon_i \tag{11}$$

where $\bar{x}_i = [x_{i,1}^\top, x_{i,2}^\top]^\top \in \mho_{\bar{x}_i}$ is an input vector with a compact set $\mho_{\bar{x}_i} \in \mathbb{R}^6$, $W_i^* = [W_{i,1}^*, \ldots, W_{i,6}^*]$ with $\|W_i^*\|_F \le \bar{W}_i$; $W_{i,l}^* = [W_{i,l,1}^*, \ldots, W_{i,l,n_l}^*]^\top$, $l = 1, \ldots, 6$, is an optimal weighting vector, $\varphi_i = [\varphi_{i,1}, \ldots, \varphi_{i,n_l}]^\top$ is a radial basis function vector, and ϵ_i is a reconstruction error vector with $\|\epsilon_i\| \le \bar{\epsilon}_i$. Here, $\bar{W}_i$ and $\bar{\epsilon}_i$ are unknown positive constants and $\|\cdot\|_F$ denotes the Frobenius norm.

The local event-triggered control law τ_i is designed as

$$\tau_i(t) = \bar{\tau}_i(t_{i,a}), \quad t \in [t_{i,a}, t_{i,a+1}), \tag{12}$$

$$t_{i,a+1} = \inf\{t > t_{i,a} | \|E_i(t)\| \ge A_{i,1}\|z_{i,2}(t)\| + A_{i,2}\}, \tag{13}$$

where $i = 1, \ldots, N$, $t_{i,a}$, $a \in \mathbb{Z}^+$, is the update time of the ith local controller, $E_i(t) = D_i(\bar{\tau}_i(t) - \tau_i(t))$, $A_{i,1} > 0$ and $A_{i,2} > 0$ are design parameters, (12) and (13) indicate that when the triggering condition $\|E_i\| \ge A_{i,1}\|z_{i,2}\| + A_{i,2}$ is satisfied, the input τ_i updates its value at $t_{i,a+1}$ and then is set to $\bar{\tau}_i(t_{i,a})$ during $t \in [t_{i,a}, t_{i,a+1})$. Here, the signal $\bar{\tau}_i$ for the event-triggered update of the control input is defined as

$$\bar{\tau}_i = D_i^{-1}\bigg(-\kappa_{i,2}z_{i,2} + M_i\dot{\bar{\nu}}_i - \hat{W}_i^\top\varphi_i - \hat{\varepsilon}_i \tanh\left(\frac{z_{i,2}}{\vartheta_{i,1}}\right) - A_{i,2}\tanh\left(\frac{z_{i,2}}{\vartheta_{i,2}}\right) - \frac{\lambda_{i,1}z_{i,2}\|z_{i,2}\|^2}{2}\bigg), \tag{14}$$

$$\dot{\hat{W}}_i = \varsigma_i(\varphi_i z_{i,2}^\top - \sigma_{i,1}\hat{W}_i), \tag{15}$$

$$\dot{\hat{\epsilon}}_i = \iota_i\left(z_{i,2}^\top \tanh\left(\frac{z_{i,2}}{\vartheta_{i,1}}\right) - \sigma_{i,2}\hat{\epsilon}_i\right), \tag{16}$$

where $i = 1, \ldots, N$, $\kappa_{i,2} = \mathrm{diag}[\kappa_{i,2,1}, \ldots, \kappa_{i,2,6}]$; $\kappa_{i,2,l} > 0$, $l = 1, \ldots, 6$, are design constants, $\tanh(z_{i,2}/\vartheta_{i,b}) = [\tanh(z_{i,2,1}/\vartheta_{i,b}), \ldots, \tanh(z_{i,2,6}/\vartheta_{i,b})]^\top$ with $b = 1, 2$ and constants $\vartheta_{i,1} > 0$ and $\vartheta_{i,2} > 0$, $\varsigma_i = \mathrm{diag}[\varsigma_{i,1}, \ldots, \varsigma_{i,6}]$; $\varsigma_{i,l} > 0$, $l = 1, \ldots, 6$, and $\iota_i > 0$ are tuning gains, and $\sigma_{i,1} > 0$ and $\sigma_{i,2} > 0$ are small constants for σ-modification [35].

Now, we consider a Lyapunov function $V_{i,2}$ as

$$V_{i,2} = V_{i,1} + \frac{1}{2}z_{i,2}^\top M_i z_{i,2} + \frac{1}{2}tr(\tilde{W}_i^\top\varsigma_i^{-1}\tilde{W}_i) + \frac{1}{2\iota_i}\tilde{\varepsilon}_i^\top\tilde{\varepsilon}_i \tag{17}$$

where $i = 1, \ldots, N$, $\tilde{\varepsilon}_i = \bar{\varepsilon}_i - \hat{\varepsilon}_i$, $\tilde{W}_i = W_i^* - \hat{W}_i$, $\hat{W}_i$ and $\hat{\epsilon}_i$ are estimates of W_i^* and $\bar{\epsilon}_i$, respectively, and $tr(\cdot)$ denotes the trace of a matrix.

By differentiating (17) with (9)–(13) and $E_i(t_{i,a}) = 0$ for $a \in \mathbb{Z}^+$, we have

$$\begin{aligned}
\dot{V}_{i,2} &= -z_{i,1}^\top\kappa_{i,1}z_{i,1} + (s_i + b_i)z_{i,1}^\top P_i(z_{i,2} + c_i) \\
&\quad + z_{i,2}^\top(\bar{G}_i + D_i\bar{\tau}_i) - z_{i,2}^\top M_i\dot{\bar{\nu}}_{i,2} - tr(\tilde{W}_i^\top\varsigma_i^{-1}\dot{\hat{W}}_i) \\
&\quad - \frac{1}{\iota_i}\tilde{\epsilon}_i^\top\dot{\hat{\epsilon}}_i - z_{i,2}^\top E_i \\
&\le -z_{i,1}^\top\kappa_{i,1}z_{i,1} + (s_i + b_i)z_{i,1}^\top P_i(z_{i,2} + c_i) \\
&\quad + z_{i,2}^\top(W_i^{*\top}\varphi_i + \epsilon_i + D_i\bar{\tau}_i) - z_{i,2}^\top M_i\dot{\bar{\nu}}_{i,2} - tr(\tilde{W}_i^\top\varsigma_i^{-1}\dot{\hat{W}}_i) \\
&\quad - \frac{1}{\iota_i}\tilde{\epsilon}_i^\top\dot{\hat{\epsilon}}_i + \|z_{i,2}\|(A_{i,1}\|z_{i,2}\| + A_{i,2}) \\
&\le -z_{i,1}^\top\kappa_{i,1}z_{i,1} + (s_i + b_i)z_{i,1}^\top P_i(z_{i,2} + c_i) \\
&\quad + z_{i,2}^\top(W_i^{*\top}\varphi_i + \epsilon_i + D_i\bar{\tau}_i) - z_{i,2}^\top M_i\dot{\bar{\nu}}_{i,2} \\
&\quad - tr(\tilde{W}_i^\top\varsigma_i^{-1}\dot{\hat{W}}_i) - \frac{1}{\iota_i}\tilde{\epsilon}_i^\top\dot{\hat{\epsilon}}_i + \frac{A_{i,1}^2}{2\lambda_{i,1}} + \frac{\lambda_{i,1}\|z_{i,2}\|^4}{2} \\
&\quad + \|z_{i,2}\|A_{i,2}
\end{aligned} \tag{18}$$

where $\lambda_{i,1} > 0$ is a design constant.

Applying (14) into (18) yields

$$\begin{aligned}
\dot{V}_{i,2} &= -z_{i,1}^\top\kappa_{i,1}z_{i,1} - z_{i,2}^\top\kappa_{i,2}z_{i,2} + (s_i + b_i)z_{i,1}^\top P_i(z_{i,2} + c_i) \\
&\quad + z_{i,2}^\top\tilde{W}_i^\top\varphi_i - tr(\tilde{W}_i^\top\varsigma_i^{-1}\dot{\hat{W}}_i) + \|z_{i,2}\|\bar{\epsilon}_i \\
&\quad - \hat{\epsilon}_i z_{i,2}^\top\tanh\left(\frac{z_{i,2}}{\vartheta_{i,1}}\right) - \frac{1}{\iota_i}\tilde{\epsilon}_i^\top\dot{\hat{\epsilon}}_i + \frac{A_{i,1}^2}{2\lambda_{i,1}} \\
&\quad + A_{i,2}\|z_{i,2}\| - A_{i,2}z_{i,2}^\top\tanh\left(\frac{z_{i,2}}{\vartheta_{i,2}}\right).
\end{aligned} \tag{19}$$

Substituting the adaptation laws (14), (15), and (16) into (19) gives

$$\begin{aligned}
\dot{V}_{i,2} &= -z_{i,1}^\top\kappa_{i,1}z_{i,1} - z_{i,2}^\top\kappa_{i,2}z_{i,2} + (s_i + b_i)z_{i,1}^\top P_i(z_{i,2} + c_i) \\
&\quad + z_{i,2}^\top\tilde{W}_i^\top\varphi_i - tr(\tilde{W}_i^\top(\varphi_i z_{i,2}^\top - \sigma_{i,1}\hat{W}_i)) \\
&\quad + \|z_{i,2}\|\bar{\epsilon}_i - \hat{\epsilon}_i z_{i,2}^\top\tanh\left(\frac{z_{i,2}}{\vartheta_{i,1}}\right) \\
&\quad - \tilde{\epsilon}_i^\top\left(z_{i,2}^\top\tanh\left(\frac{z_{i,2}}{\vartheta_{i,1}}\right) - \sigma_{i,2}\hat{\epsilon}_i\right) \\
&\quad + A_{i,2}\left(\|z_{i,2}\| - z_{i,2}^\top\tanh\left(\frac{z_{i,2}}{\vartheta_{i,2}}\right)\right) + \frac{A_{i,1}^2}{2\lambda_{i,1}}.
\end{aligned} \tag{20}$$

Lemma 1 [34]: For any $\vartheta > 0$ and $z \in \mathbb{R}$, it holds that $0 \le |z| - z\tanh(z/\vartheta) \le 0.2785\vartheta$.

From the definitions $z_{i,2} = [z_{i,2,1}, \ldots, z_{i,2,6}]^\top$ and $\tanh(z_{i,2}/\vartheta_{i,b}) = [\tanh(z_{i,2,1}/\vartheta_{i,b}), \ldots, \tanh(z_{i,2,6}/\vartheta_{i,b})]^\top$ for $b = 1, 2$, using Lemma 1 yields

$$\begin{aligned}
&\|z_{i,2}\| - z_{i,2}^\top\tanh\left(\frac{z_{i,2}}{\vartheta_{i,b}}\right) \\
&\le \sum_{l=1}^{6}\left(|z_{i,2,l}| - z_{i,2,l}\tanh\left(\frac{z_{i,2,l}}{\vartheta_{i,b}}\right)\right) \le 1.671\vartheta_{i,b}.
\end{aligned} \tag{21}$$

Thus, it is obtained that

$$\|z_{i,2}\|\bar{\epsilon}_i \le \bar{\epsilon}_i z_{i,2}^\top\tanh\left(\frac{z_{i,2}}{\vartheta_{i,1}}\right) + 1.671\bar{\epsilon}_i\vartheta_{i,1}, \tag{22}$$

$$\|z_{i,2}\| \leq z_{i,2}^{\top} \tanh\left(\frac{z_{i,2}}{\vartheta_{i,2}}\right) + 1.671\vartheta_{i,2}. \tag{23}$$

Based on the cyclic nature of the trace, $\dot{V}_{i,2}$ becomes

$$\begin{aligned}\dot{V}_{i,2} \leq & -z_{i,1}^{\top}\kappa_{i,1}z_{i,1} - z_{i,2}^{\top}\kappa_{i,2}z_{i,2} + (s_i+b_i)z_{i,1}^{\top}P_i(z_{i,2}+c_i) \\ & + \sigma_{i,1}tr(\tilde{W}_i^{\top}\hat{W}_i) + \sigma_{i,2}\tilde{\epsilon}_i^{\top}\hat{\epsilon}_i + \frac{A_{i,1}^2}{2\lambda_{i,1}} \\ & + 1.671\bar{\epsilon}_{i,1}\vartheta_{i,1} + 1.671A_{i,2}\vartheta_{i,2}. \end{aligned} \tag{24}$$

Remark 3: Compared with the existing works [8]–[10], [14], [15] for single stratospheric airships, the proposed control scheme (13)–(16) deals with the distributed formation control problem for networked multiple stratospheric airships and the local controller (12) updates its value according to the proposed asynchronous triggering rule (13). Although the local controllers (12) are intermittently updated and the leader output signal is only available for some of the followers, the stability of the resulting formation control system can be ensured, as presented in the following section.

Remark 4: Using $\tau_i = [\tau_{i,1}, \ldots, \tau_{i,6}]^{\top}$, the practical control inputs $T_{i,L}$, $T_{i,R}$, $\mu_{i,L}$, $\mu_{i,R}$, $\delta_{i,E}$, and $\delta_{i,L}$ can be easily computed as $T_{i,L} = \sqrt{\tau_{i,4}^2 + \tau_{i,6}^2}$, $T_{i,R} = \sqrt{\tau_{i,5}^2 + \tau_{i,1}^2}$, $\mu_{i,L} = \arctan(\tau_{i,6}/\tau_{i,4})$, $\mu_{i,R} = \arctan(\tau_{i,1}/\tau_{i,5})$, $\delta_{i,R} = \tau_{i,2}$, and $\delta_{i,E} = \tau_{i,3}$.

B. STABILITY ANALYSIS

The dynamics of the boundary layer error c_i is obtained as

$$\dot{c}_i = -\frac{c_i}{\xi_i} + \Gamma_i(z_{i,1}, z_{i,2}, c_i, z_{l,1}, z_{l,2}, c_l, \hat{W}_l, \hat{\epsilon}_l, \Omega_0) \tag{25}$$

where $i = 1, \ldots, N$, $l \in \mathcal{N}_i$, $l = 1, \ldots, N$, $\Omega_0 = [\varpi_0^{\top}, \dot{\varpi}_0^{\top}, \ddot{\varpi}_0^{\top}]^{\top}$, and $\Gamma_i(\cdot) = (1/(s_i+b_i))\dot{P}_i^{-1}[\kappa_{i,1}z_{i,1} - \sum_{j=1}^{N} h_{i,j}P_jx_{j,2} - s_i\dot{\varpi}_0] + (1/(s_i+b_i))P_i^{-1}[\kappa_{i,1}\dot{z}_{i,1} - \sum_{j=1}^{N} h_{i,j} \times(\dot{P}_jx_{j,2} + P_j\dot{x}_{j,2}) - s_i\ddot{\varpi}_0]$ is a continuous function.

Then, consider a total Lyapunov function V as

$$V = \sum_{i=1}^{N}\left[V_{i,2} + \frac{1}{2}c_i^{\top}c_i\right]. \tag{26}$$

Theorem 1: Consider the networked multiple stratospheric airships (4) with unknown nonlinearities under the directed graph. For all initial conditions that satisfy $V(0) \leq \Delta$, the proposed event-triggered adaptive formation tracker (i.e., (12)–(16)) with event-triggering laws (13) ensures that

(i) all the closed-loop signals are semi-globally uniformly ultimately bounded;
(ii) $\lim_{t\to\infty}\|\varpi - (1_N \otimes \varpi_0) - \bar{o}\| \leq \breve{\varepsilon}$;
(iii) there exist minimum inter-event times $t_i^* > 0$ such that $|t_{i,a+1} - t_{i,a}| \geq t_i^*$

where $i = 1, \ldots, N$, $\varpi = [\varpi_1^{\top}, \ldots, \varpi_N^{\top}]^{\top}$, 1_N is an N-vector of all ones, $\otimes$ indicates the Kronecker product, $\bar{o} = [\bar{o}_{1,0}^{\top}, \ldots, \bar{o}_{N,0}^{\top}]^{\top}$, $\breve{\varepsilon} > 0$ is a constant that can be made arbitrarily small, and t_i^* is the minimum inter-execution time.

Proof: From (24) and (25), the time derivative of V becomes

$$\begin{aligned}\dot{V} \leq \sum_{i=1}^{N}\Big[& -z_{i,1}^{\top}\kappa_{i,1}z_{i,1} - z_{i,2}^{\top}\kappa_{i,2}z_{i,2} - \frac{1}{\xi_i}c_i^{\top}c_i \\ & + c_i^{\top}\Gamma_i + (s_i+b_i)z_{i,1}^{\top}P_i(z_{i,2}+c_i) \\ & + \sigma_{i,1}tr(\tilde{W}_i^{\top}\hat{W}_i) \\ & - \sigma_{i,2}\tilde{\epsilon}_i^2 + \sigma_{i,2}\tilde{\epsilon}_i\bar{\epsilon}_i + \frac{A_{i,1}^2}{2\lambda_{i,1}} \\ & + 1.671\bar{\epsilon}_{i,1}\vartheta_{i,1} + 1.671A_{i,2}\vartheta_{i,2}\Big]. \end{aligned} \tag{27}$$

Using Young's inequality[1], it holds that

$$\begin{aligned}(s_i+b_i)z_{i,1}^{\top}P_i(z_{i,2}+c_i) &\leq \frac{(s_i+b_i)^2}{2}\|P_i\|^2\|z_{i,1}\|^2 \\ &\quad + \|z_{i,2}\|^2 + \|c_i\|^2, \\ tr(\tilde{W}_i^{\top}\hat{W}_i) &= \|\tilde{W}_i\|_F\bar{W}_i - \|\tilde{W}_i\|_F^2 \\ &\leq -\frac{1}{2}\|\tilde{W}_i\|_F^2 + \frac{1}{2}\bar{W}_i^2, \\ \tilde{\epsilon}_i\bar{\epsilon}_i &\leq \frac{1}{2}\tilde{\epsilon}_i^2 + \frac{1}{2}\bar{\epsilon}_i^2, \\ c_i^{\top}\Gamma_i &\leq \frac{\|c_i\|^2\|\Gamma_i\|^2}{2\lambda_{i,2}} + \frac{\lambda_{i,2}}{2}, \end{aligned}$$

where $\lambda_{i,2}$ are positive constants.

From the above inequalities, (27) becomes

$$\begin{aligned}\dot{V} \leq \sum_{i=1}^{N}\Big[& -z_{i,1}^{\top}\kappa_{i,1}z_{i,1} - z_{i,2}^{\top}\kappa_{i,2}z_{i,2} - \frac{\|c_i\|^2}{\xi_i} + \frac{\|c_i\|^2\|\Gamma_i\|^2}{2\lambda_{i,2}} \\ & + \frac{(s_i+b_i)^2}{2}\|P_i\|^2\|z_{i,1}\|^2 + \|z_{i,2}\|^2 + \|c_i\|^2 \\ & - \frac{\sigma_{i,1}}{2}\|\tilde{W}_i\|_F^2 - \frac{\sigma_{i,2}}{2}\|\tilde{\epsilon}_i\|^2\Big] + C \end{aligned} \tag{28}$$

where $C = \sum_{i=1}^{N}[(\sigma_{i,1}/2)\bar{W}_i^2 + (\sigma_{i,2}/2)\bar{\epsilon}_i^2 + \lambda_{i,2}/2 + A_{i,1}^2/(2\lambda_{i,1}) + 1.671\bar{\epsilon}_{i,1}\vartheta_{i,1} + 1.671\,A_{i,2}\vartheta_{i,2}]$.

Define two compact sets $\Pi_i = \{z_{i,1}^{\top}z_{i,1} + z_{i,2}^{\top}z_{i,2} + c_i^{\top}c_i + \sum_{l\in\mathcal{N}_i}[z_{l,1}^{\top}z_{l,1} + z_{l,2}^{\top}z_{l,2} + c_l^{\top}c_l + tr(\tilde{W}_l^{\top}\varsigma_l^{-1}\tilde{W}_l) + (1/\iota_l)\tilde{\epsilon}_l^2] \leq 2\Delta\}$ and $\Xi = \{\varpi_0^{\top}\varpi_0 + \dot{\varpi}_0^{\top}\dot{\varpi}_0 + \ddot{\varpi}_0^{\top}\ddot{\varpi}_0 \leq \bar{\Omega}_0\}$ where $i = 1, \ldots, N$ and $\bar{\Omega}_0 > 0$ is a constant. Since Π_i and Ξ are compact sets, $\Pi_i \times \Xi$ is also a compact set. Therefore, there exists a constant $\bar{\Gamma}_i$ such that $\|\Gamma_i\| \leq \bar{\Gamma}_i$ on $\Pi_i \times \Xi$.

Based on this fact and selecting the design parameters as $\kappa_{i,1} = (1/2)(s_i+b_i)^2\|P_i\|^2I + \kappa_{i,1}^*I$, $\kappa_{i,2} = I + \kappa_{i,2}^*I$, and $1/\xi_i = \xi_i^* + \bar{\Gamma}_i^2/(2\lambda_{i,2}) + 1$ with an identity matrix $I \in \mathbb{R}^{6\times 6}$ and positive constants $\kappa_{i,1}^*$, $\kappa_{i,2}^*$, and ξ_i^*, (28) can be represented by

$$\dot{V} \leq -\Upsilon V - \left(1 - \frac{\|\Gamma\|_i^2}{\bar{\Gamma}_i^2}\right)\frac{\|c_i\|\bar{\Gamma}_i^2}{2\lambda_i} + C \tag{29}$$

where $\Upsilon = \min[2\kappa_{i,1}^*, 2\kappa_{i,2}^*, 2\xi_i^*, \sigma_{i,1}\varsigma_{i,m}, \sigma_{i,2}\iota_i]$ with $i = 1, \ldots, N$ and $\varsigma_{i,m}$ are the minimum eigenvalues of ς_i. The

[1] $ab \leq \frac{a^p}{p} + \frac{b^q}{q}$ where $a, b \geq 0$ and $p, q > 0$ such that $1/p + 1/q = 1$.

above inequality becomes $\dot{V} \leq -\Upsilon V + C$ on $V = \Delta$. This means that $\dot{V} < 0$ on $V = \Delta$ when $\Upsilon > C/\Delta$. Therefore, $V \leq \Delta$ is an invariant set, i.e, if $V(0) \leq \Delta$, then $V(t) \leq \Delta$ for all $t \geq 0$. Integrating the both sides of $\dot{V} \leq -\Upsilon V + C$ with respect to time, we have $V(t) \leq e^{-\Upsilon t}V(0) + (C/\Upsilon)[1 - e^{-\Upsilon t}]$. By considering this inequality and defining a constant Ψ to satisfy $\Psi > C/\Upsilon$, it is guaranteed that for all $\varphi \in (0, \Delta)$, there exists $T \geq 0$ such that $\|V(0)\| \leq \varphi \Rightarrow \|V(t)\| \leq \Psi$ for all $t \geq T$. Thus, Definition 1 ensures that all the closed-loop signals are semi-globally uniformly ultimately bounded. This completes the proof of Theorem 1–(i).

Additionally, we have $(1/2)\|z_1\|^2 \leq V(t)$. Thus, it holds that $\lim_{t\to\infty} \|z_1(t)\| \leq \sqrt{2C/\Upsilon}$ where $\sqrt{2C/\Upsilon}$ can be reduced arbitrarily small by increasing Υ or decreasing C (i.e., by adjusting the design parameters). Then, z_1 is represented by $z_1 = ((\bar{\mathscr{L}} + \mathscr{S}) \otimes I)(\varpi - (1_N \otimes \varpi_0) - \bar{o})$. From Assumption 3, $\bar{\mathscr{L}} + \mathscr{S}$ is invertible. Therefore, it holds that $\lim_{t\to\infty} \|\varpi - (1_N \otimes \varpi_0) - \bar{o}\| \leq \check{\varepsilon}$ where $\check{\varepsilon} = \sqrt{2C/\Upsilon}\|((\bar{\mathscr{L}} + \mathscr{S}) \otimes I)^{-1}\|$. Since $\sqrt{2C/\Upsilon}$ can be reduced arbitrarily small, $\check{\varepsilon}$ can also be made arbitrarily small. This completes the proof of Theorem 1–(ii).

To avoid the Zeno behavior denoting an infinite number of triggering instants in a finite time, we show that there exist minimum inter-event times t_i^* that satisfy $|t_{i,a+1} - t_{i,a}| \geq t_i^*$ for $a \in \mathbb{Z}^+$. The time derivatives of the measurement errors $E_i(t)$, $\forall t \in [t_{i,a}, t_{i,a+1})$, are given by $\frac{d}{dt}\|E_i\| = \frac{d}{dt}(E_i^\top E_i)^{\frac{1}{2}} = \frac{E_i^\top \dot{E}_i}{\|E_i\|} \leq \|\frac{d}{dt}(D_i\bar{\tau}_i)\|$. $\frac{d}{dt}(D_i\bar{\tau}_i)$ is given by

$$\begin{aligned}\frac{d}{dt}(D_i\bar{\tau}_i) = &-\kappa_{i,2}\dot{z}_{i,2} + M_i\ddot{\bar{v}}_i - \dot{\hat{W}}_i^\top\varphi_i - \hat{W}_i^\top\dot{\varphi}_i \\ &- \dot{\hat{\varepsilon}}_i \tanh\left(\frac{z_{i,2}}{\vartheta_{i,1}}\right) - \hat{\varepsilon}_i\left(1 - \tanh^2\left(\frac{z_{i,2}}{\vartheta_{i,1}}\right)\right)\frac{\dot{z}_{i,2}}{\vartheta_{i,1}} \\ &- A_{i,2}\left(1 - \tanh^2\left(\frac{z_{i,2}}{\vartheta_{i,2}}\right)\right)\frac{\dot{z}_{i,2}}{\vartheta_{i,2}} \\ &- \frac{\lambda_{i,1}\dot{z}_{i,2}\|z_{i,2}\|^2}{2} - \lambda_{i,1}z_{i,2}\|z_{i,2}\|\dot{z}_{i,2}. \end{aligned} \tag{30}$$

Since all the signals of the closed-loop system are bounded, there is a constant $\gamma_i > 0$ such that $\|\frac{d}{dt}(D_i\bar{\tau}_i)\| \leq \gamma_i$. Integrating $\frac{d}{dt}\|E_i\| \leq \gamma_i$ during $t \in [t_{i,a}, t_{i,a+1})$ and using the event-triggering condition (13) yield $|t_{i,a+1} - t_{i,a}| \geq (A_{i,1}\|z_{i,2}(t)\| + A_{i,2})/\gamma_i \geq A_{i,2}/\gamma_i$. Therefore, it holds that $|t_{i,a+1} - t_{i,a}| \geq t_i^*$ with $t_i^* = A_{i,2}/\gamma_i$. This completes the proof of Theorem 1–(iii). ■

Remark 5: The design parameters of the distributed event-triggered adaptive formation tracking laws can be selected based on the proof result of Theorem 1. The guidelines for selecting design parameters are as follows:

1) Increasing $\kappa_{i,1}$ and $\kappa_{i,2}$ and decreasing ξ_i with $i = 1, \ldots, N$ result in increasing Υ which subsequently reduce the convergence bound $\sqrt{2C/\Upsilon}$ of $z_{i,1}$.

2) Decreasing $\vartheta_{i,1}$ and $\vartheta_{i,2}$ assists in decreasing C. Then, the bound $\sqrt{2C/\Upsilon}$ of the tracking error $z_{i,1}$ can be reduced.

3) Selecting $\sigma_{i,1}$ and $\sigma_{i,2}$ as small constants and increasing ι_i and ς_i are desirable to increase the tuning speed of the adaptive parameters $\hat{W}_i$ and $\hat{\epsilon}_i$.

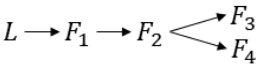

FIGURE 2. Directed network topology.

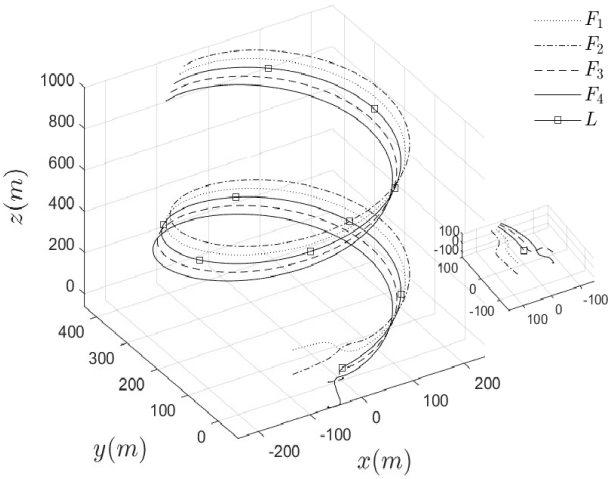

FIGURE 3. Distributed formation tracking results.

4) Adjusting $A_{i,1}$ and $A_{i,2}$ helps to adjust the number of released data according to the limited resources of the network in the transient and steady-state response, respectively.

IV. SIMULATION RESULTS

Consider a group consisting of a leader (i.e., L) and four airship followers (i.e., $F_1, \ldots, F_4$) described by system (4) where the event-triggering condition (13) is monitored periodically with the sampling period 0.001 sec. The system parameters and coefficients are presented in Table 1 [10]. The dynamic leader signal vector is defined as $\varpi_0(t) = [200\sin(0.1t), 200 - 200\cos(0.1t), 10t, 0, -0.464, 0.01t]^\top$. The directed network topology for one leader and four airship followers is given in Fig. 2 where $h_{2,1} = h_{3,2} = h_{4,2} = 1$, $h_{1,2} = h_{1,3} = h_{1,4} = h_{2,3} = h_{2,4} = h_{3,1} = h_{3,4} = h_{4,1} = h_{4,3} = 0$, $s_1 = 1$, and $s_2 = s_3 = s_4 = 0$. For the

TABLE 1. System parameters and coefficients.

Parameter	Value	Unit	Coefficient	Value
m_i	5.6×10^3	kg	$k_{i,1}$	0.17
$\bigwedge_i$	7.4×10^5	m^3	$k_{i,2}$	0.83
ρ_i	0.089	kg/m^3	$k_{i,3}$	0.52
$x_{i,g}$	5	m	$C_{i,X1}$,$C_{i,X2}$	657
$z_{i,g}$	15	m	$C_{i,Y1} \ldots C_{i,Y4}$	657
$x_{i,p}$	4	m	$C_{i,Z1} \ldots C_{i,Z4}$	657
$y_{i,p}$	0.5	m	$C_{i,L1}$	2.4×10^4
$z_{i,p}$	40	m	$C_{i,N1} \ldots C_{i,N4}$	7.7×10^4
$I_{i,x}$	5×10^7	$kg \cdot m^2$	$C_{i,M1} \ldots C_{i,M4}$	7.7×10^4
$I_{i,y}$	2.9×10^8	$kg \cdot m^2$		
$I_{i,z}$	2.9×10^8	$kg \cdot m^2$		
$I_{i,xz}$	-6×10^4	$kg \cdot m^2$		
χ_i	$\pi/6$	m		
g	9.8	m/s^2		

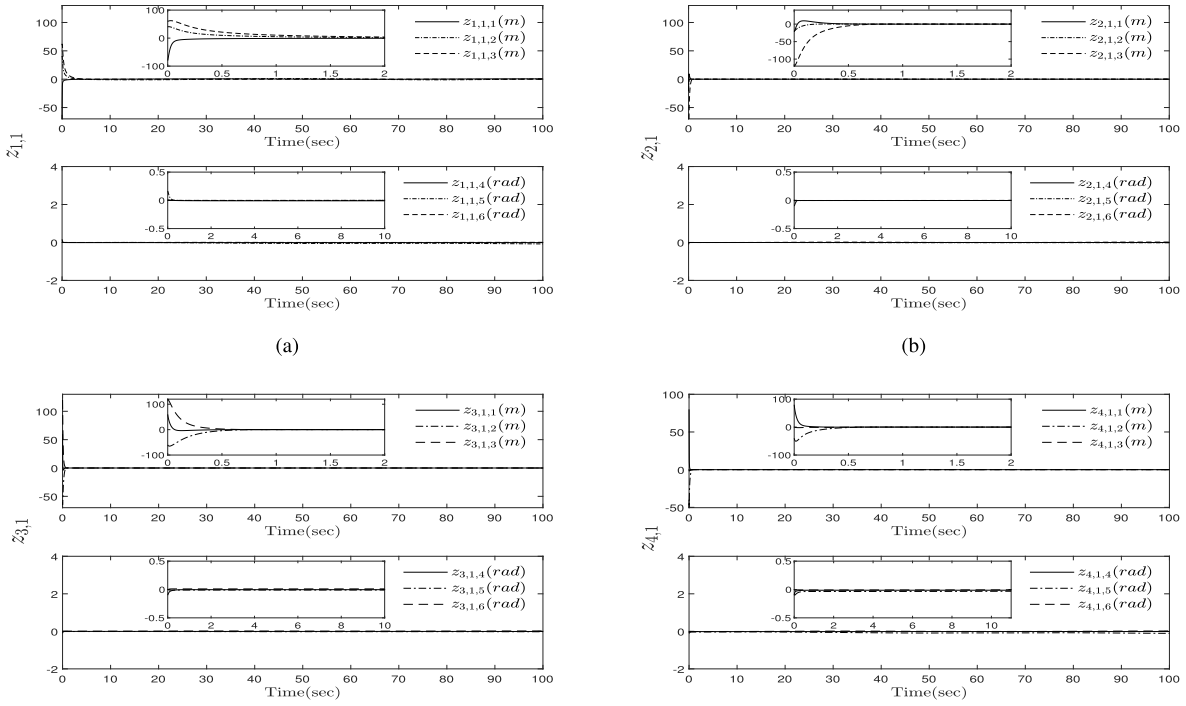

FIGURE 4. Formation tracking errors (a) $z_{1,1}$ (b) $z_{2,1}$ (c) $z_{3,1}$ (d) $z_{4,1}$.

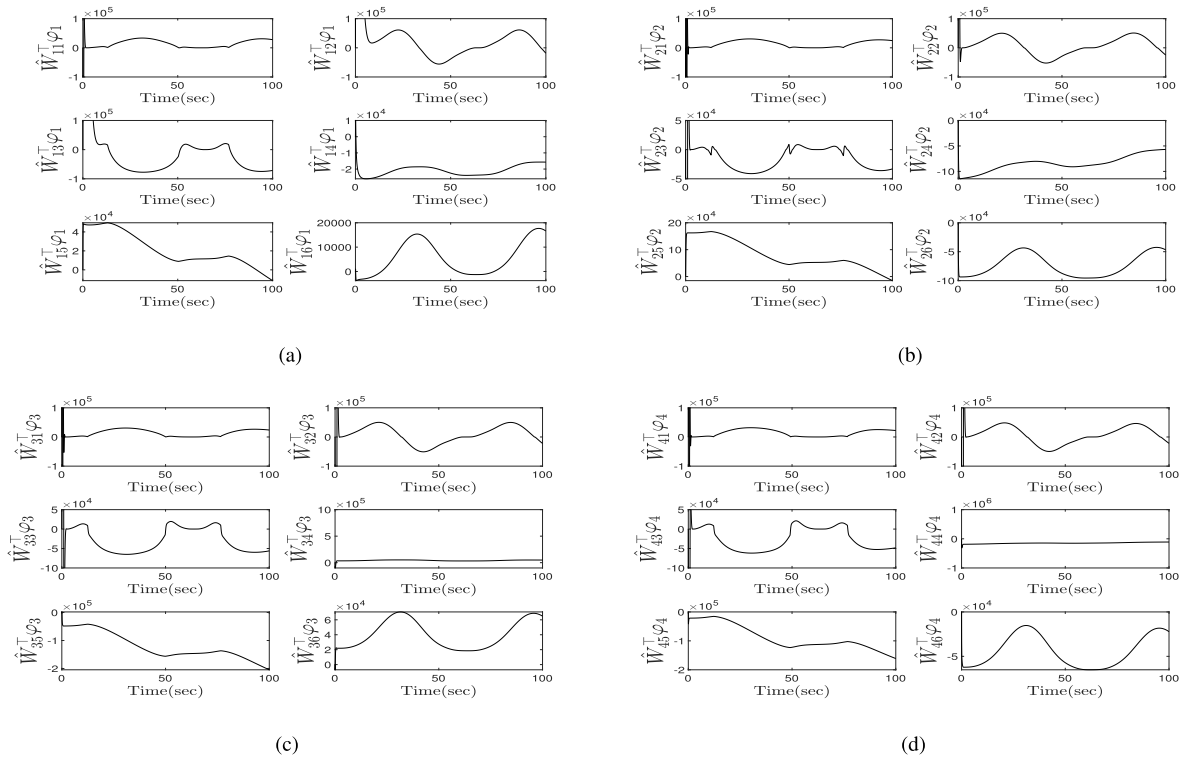

FIGURE 5. The outputs of radial basis function neural networks (a) $\hat{W}_1^{\top}\varphi_1$ (b) $\hat{W}_2^{\top}\varphi_2$ (c) $\hat{W}_3^{\top}\varphi_3$ (d) $\hat{W}_4^{\top}\varphi_4$.

simulation, the desired offsets among the followers and the leader are set to $\bar{o}_{1,0} = [-10, -10, -10, 0, 0, 0]^{\top}$, $\bar{o}_{2,1} = [0, 0, -20, 0, 0, 0]^{\top}$, $\bar{o}_{3,2} = [-20, -20, 20, 0, 0, 0]^{\top}$, and $\bar{o}_{4,2} = [0, 0, -20, 0, 0, 0]^{\top}$. The initial conditions of airship followers are $x_1(0) = [-60, 60, 60, 0, -0.3, 0]$, $x_2(0) = [-60, 60, -60, 0, -0.3, -0.1]$, $x_3(0) = [60, -60, 60,$

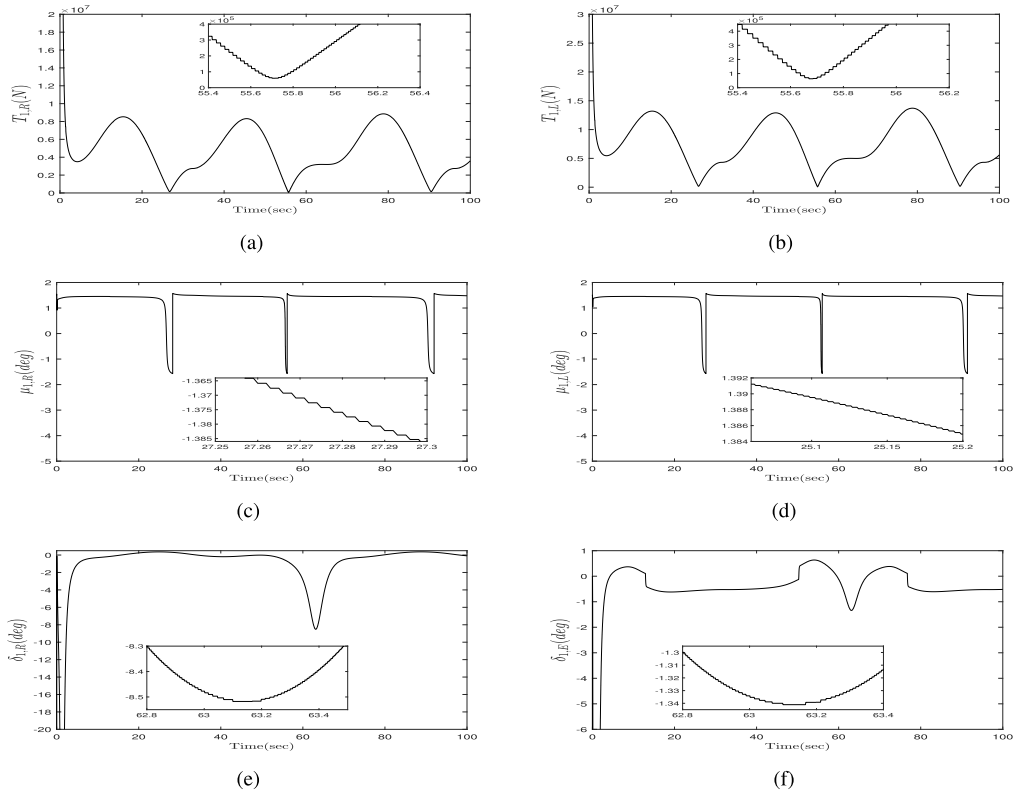

FIGURE 6. Control inputs of F_1 (a) $T_{1,R}$ (b) $T_{1,L}$ (c) $\mu_{1,R}$ (d) $\mu_{1,L}$ (e) $\delta_{1,R}$ (f) $\delta_{1,E}$.

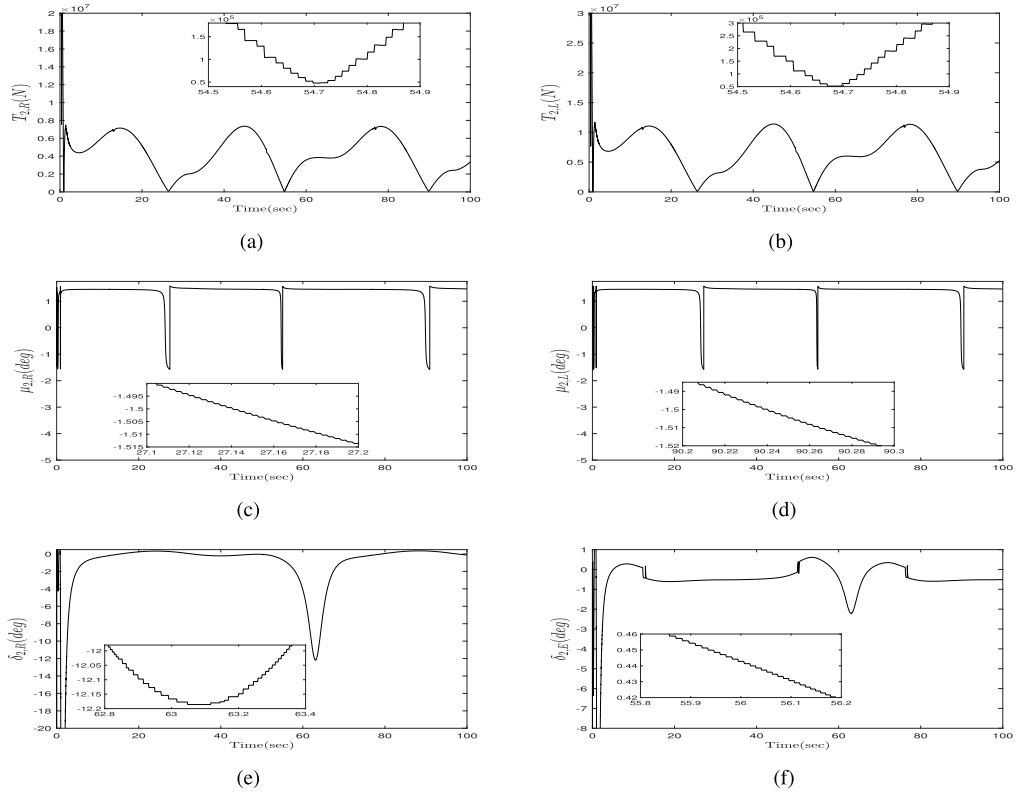

FIGURE 7. Control inputs of F_2 (a) $T_{2,R}$ (b) $T_{2,L}$ (c) $\mu_{2,R}$ (d) $\mu_{2,L}$ (e) $\delta_{2,R}$ (f) $\delta_{2,E}$.

$-0.1, -0.3, -0.1]$, and $x_4(0) = [-60, -60, -60, -0.1, -0.4, -0.1]$ and the design parameters of airship followers are chosen as $\kappa_{1,1} = \text{diag}[50, 15, 15, 60, 13, 70]$, $\kappa_{2,1} = \text{diag}[35, 15, 15, 60, 60, 17]$, $\kappa_{3,1} = \text{diag}[35, 15, 15, 35, 60, 40]$, and $\kappa_{4,1} = \text{diag}[35, 30, 30, 70, 7, 15]$, $\kappa_{i,2} = \text{diag}[23, 20, 20, 10, 10, 10]$, $\varsigma_{i,l} = 2 \times 10^5$, $\sigma_{i,1} = 10^{-5}$,

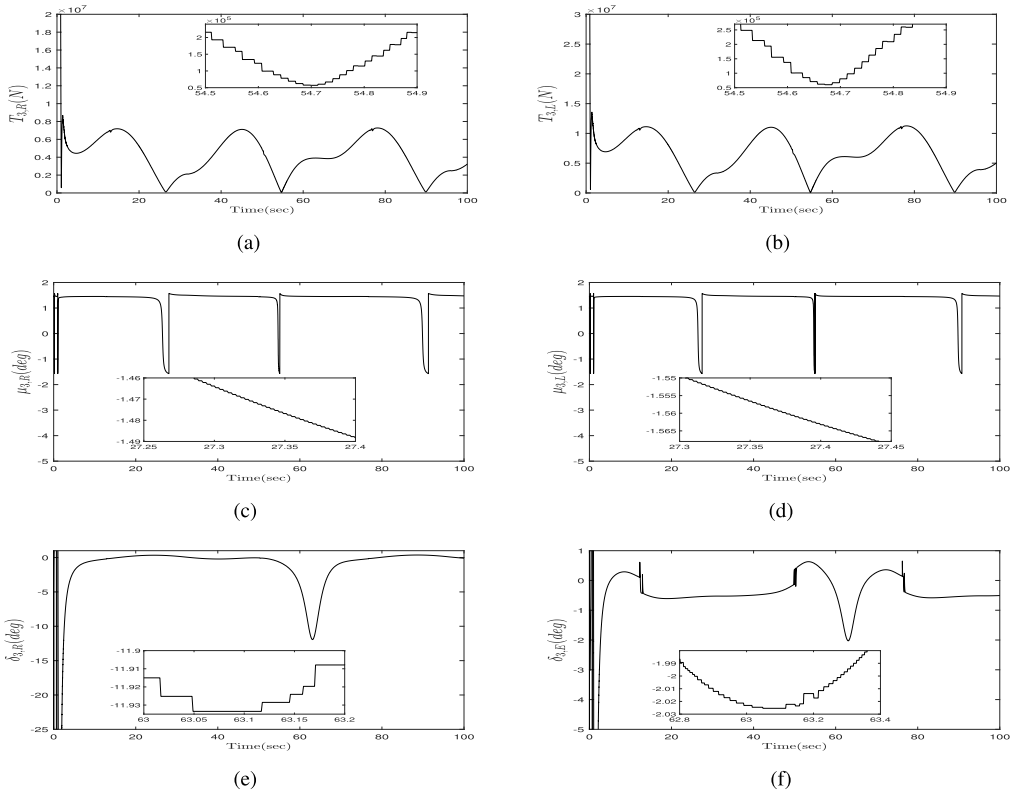

FIGURE 8. Control inputs of F_3 (a) $T_{3,R}$ (b) $T_{3,L}$ (c) $\mu_{3,R}$ (d) $\mu_{3,L}$ (e) $\delta_{3,R}$ (f) $\delta_{3,E}$.

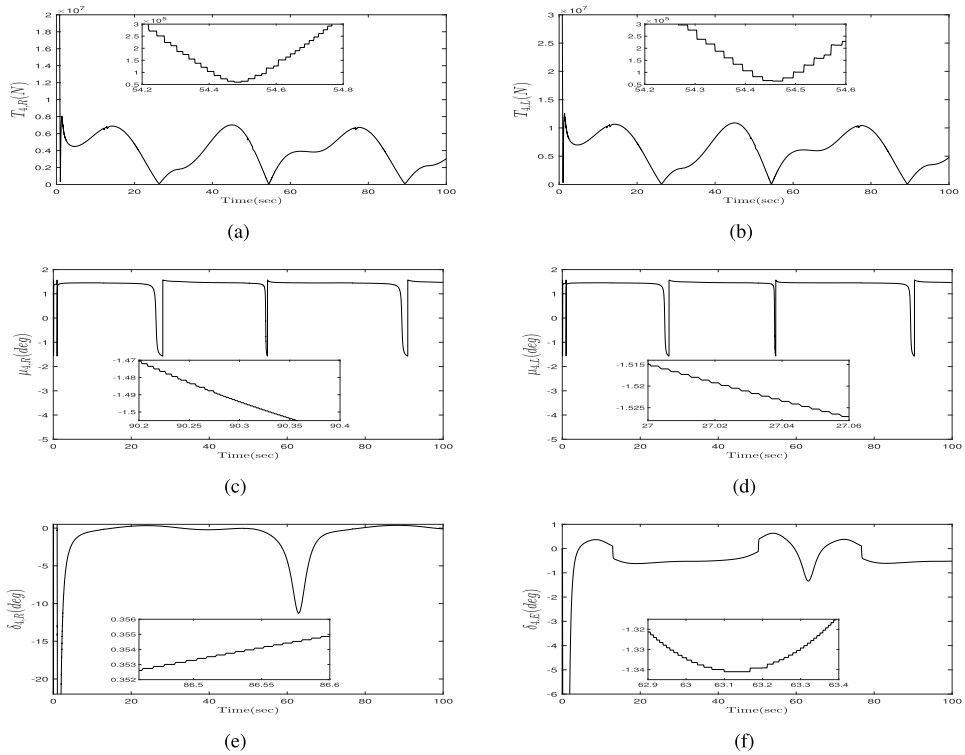

FIGURE 9. Control inputs of F_4 (a) $T_{4,R}$ (b) $T_{4,L}$ (c) $\mu_{4,R}$ (d) $\mu_{4,L}$ (e) $\delta_{4,R}$ (f) $\delta_{4,E}$.

$\sigma_{i,2} = 1$, $\iota_i = 1$, $\xi_i = 10^{-3}$, $\vartheta_{i,1} = 10^{-2}$, $\vartheta_{i,2} = 10^{-2}$, $\lambda_{i,1} = 1$, $A_{1,1} = A_{2,1} = A_{3,1} = A_{4,1} = 500$, $A_{1,2} = A_{2,2} = A_{3,2} = A_{4,2} = 1000$, $u_{i,\omega} = 10$, $v_{i,\omega} = 10$, and $w_{i,\omega} = 10$ where $i = 1, \ldots, 4$ and $l = 1, \ldots, 6$.

Fig. 3 shows the formation tracking results in the three-dimensional space. The formation control errors for the positions and attitudes of the airship followers are displayed in Fig. 4 where $z_{i,1} = [z_{i,1,1}, \ldots, z_{i,1,6}]^\top$ with $i = 1, \ldots, 4$.

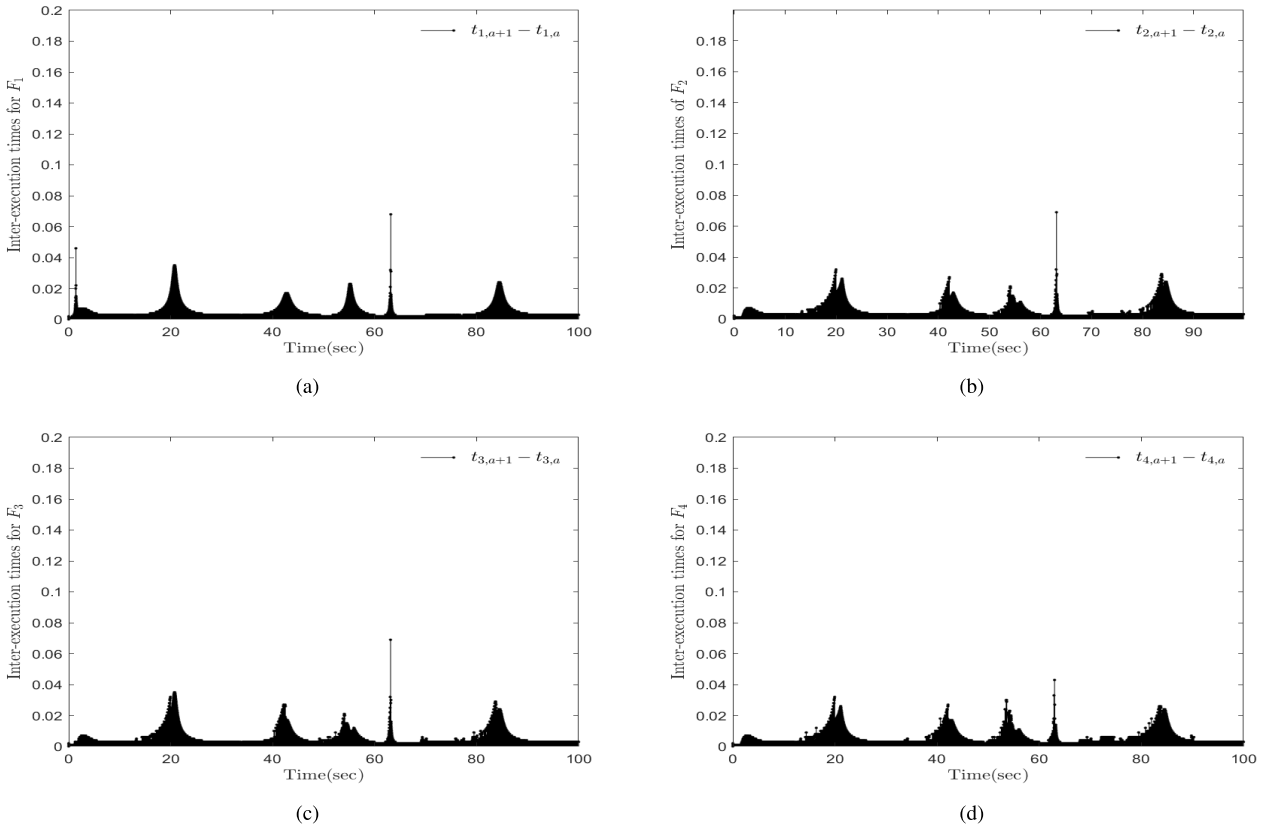

FIGURE 10. Inter-execution times (a) Inter-execution times for F_1 (b) Inter-execution times for F_2 (c) Inter-execution times for F_3 (d) Inter-execution times for F_4.

These figures reveal that the formation tracking errors quickly converge to a vicinity of zero in less than a few seconds. The outputs of the employed radial basis function neural networks and the event-triggered input signals $T_{i,R}$, $T_{i,L}$, $\mu_{i,R}$, $\mu_{i,L}$, $\delta_{i,R}$, and $\delta_{i,E}$ with $i = 1, \ldots, 4$ are plotted in Figs. 5 and 6–9, respectively. The inter-execution times are displayed in Fig. 10. The total event numbers are 29563 for F_1, 29044 for F_2, 28828 for F_3, and 27349 for F_4. Thus, only 29.593%, 29.044%, 28.828%, and 27.394% of the total data 10^5 sampled during 100 sec are only required to implement the local control laws for the airship followers. From these figures, we can conclude that the distributed formation control of networked uncertain stratospheric airships can be successfully achieved under the proposed event-triggered formation tracking scheme although the system nonlinearities are unknown and local event-triggered control inputs are used.

V. CONCLUSION

This paper has investigated the distributed event-triggered adaptive control strategy to solve the formation tracking problem of networked uncertain stratospheric airships. The local event-triggered adaptive formation tracker has been designed to obtain the desired formations for both the positions and attitudes of uncertain stratospheric airship followers where asynchronous event-triggering laws are derived to update local control laws intermittently in time. It has shown that the proposed formation tracking algorithm ensures the stability of the resulting closed-loop system and prevents the Zeno behavior, while dealing effectively with the effects of the unknown heterogeneous nonlinearities of the airship followers. Finally, the effectiveness of the proposed control system has been validated using simulation results. Further studies on the output-feedback formation tracking problem of networked uncertain stratospheric airships can be recommended as future works.

REFERENCES

[1] J. A. Roney, "Statistical wind analysis for near-space applications," *J. Atmos. Sol.-Terr. Phys.*, vol. 69, no. 13, pp. 1485–1501, Sep. 2007.
[2] W.-Q. Wang, "Near-space vehicles: Supply a gap between satellites and airplanes for remote sensing," *IEEE Aerosp. Electron. Syst. Mag.*, vol. 26, no. 4, pp. 4–9, Apr. 2011.
[3] C.-H. Won, "Regional navigation system using geosynchronous satellites and stratospheric airships," *IEEE Trans. Aerosp. Electron. Syst.*, vol. 38, no. 1, pp. 271–278, Jan. 2002.
[4] I. Schafer and K. Reimund, "Airships as unmanned platforms: Challenge and chance," in *Proc. AIAA Tech. Conf. Workshop Unmanned Aerosp. Veh.*, Portsmouth, VA, USA, 2008, pp. 1–9.
[5] G. H. Khoury and J. D. Gillett, *Airship Technology*. Cambridge, U.K.: Cambridge Univ. Press, 1999.
[6] Y. Yang and Y. Yan, "Neural network approximation-based nonsingular terminal sliding mode control for trajectory tracking of robotic airships," *Aerosp. Sci. Technol.*, vol. 54, pp. 192–197, Jul. 2016.

[7] A. Moutinho and J. R. Azinheira, "Stability and robustness analysis of the AURORA airship control system using dynamic inversion," in *Proc. IEEE Int. Conf. Robot. Automat.*, Barcelona, Spain, 2005, pp. 2265–2270.
[8] Z. Zuo, L. Cheng, X. Wang, and K. Sun, "Three dimensional path following backstepping control for an underactuated stratospheric airship," *IEEE Trans. Aero. Electron. Syst.*, vol. 55, no. 3, pp. 1483–1497, Jun. 2019.
[9] Z. Zheng, M. Feroskhan, and L. Sun, "Adaptive fixed-time trajectory tracking control of a stratospheric airship," *ISA Trans.*, vol. 76, pp. 134–144, May 2018.
[10] L. Sun and Z. Zheng, "Nonlinear adaptive trajectory tracking control for a stratospheric airship with parametric uncertainty," *Nonlinear Dyn.*, vol. 82, no. 3, pp. 1419–1430, Nov. 2015.
[11] S. He, H. Fang, M. Zhang, F. Liu, and Z. Ding, "Adaptive optimal control for a class of nonlinear systems: The online policy iteration approach," *IEEE Trans. Neural Netw. Learn. Syst.*, vol. 31, no. 2, pp. 549–558, Feb. 2020.
[12] S. He, H. Fang, M. Zhang, F. Liu, X. Luan, and Z. Ding, "Online policy iterative-based H_∞ optimization algorithm for a class of nonlinear systems," *Inform. Sci.*, vol. 495, pp. 1–13, Aug. 2019.
[13] S. He, M. Zhang, H. Fang, F. Liu, X. Luan, and Z. Ding, "Reinforcement learning and adaptive optimization of a class of Markov jump systems with completely unknown dynamic information," *Neur. Comp. Appl.*, 2019, doi: 10.1007/s00521-019-04180-2.
[14] Z. Zheng and Y. Zou, "Adaptive integral LOS path following for an unmanned airship with uncertainties based on robust RBFNN backstepping," *ISA Trans.*, vol. 65, pp. 210–219, Nov. 2016.
[15] W. Lou, M. Zhu, X. Guo, and H. Liang, "Command filtered sliding mode trajectory tracking control for unmanned airships based on RBFNN approximation," *Adv. Space Res.*, vol. 63, no. 3, pp. 1111–1121, Feb. 2019.
[16] A. Girard, "Dynamic triggering mechanisms for event-triggered control," *IEEE Trans. Autom. Control*, vol. 60, no. 7, pp. 1992–1997, Jul. 2015.
[17] W. P. M. H. Heemels, M. C. F. Donkers, and A. R. Teel, "Periodic event-triggered control for linear systems," *IEEE Trans. Autom. Control*, vol. 58, no. 4, pp. 847–861, Apr. 2013.
[18] S. Hu and D. Yue, "Event-triggered control design of linear networked systems with quantizations," *ISA Trans.*, vol. 51, no. 1, pp. 153–162, Jan. 2012.
[19] T. Henningsson, E. Johannesson, and A. Cervin, "Sporadic event-based control of first-order linear stochastic systems," *Automatica*, vol. 44, no. 11, pp. 2890–2895, Nov. 2008.
[20] P. Tabuada, "Event-triggered real-time scheduling of stabilizing control tasks," *IEEE Trans. Autom. Control*, vol. 52, no. 9, pp. 1680–1685, Sep. 2007.
[21] M. Mazo and P. Tabuada, "Decentralized event-triggered control over wireless sensor/actuator networks," *IEEE Trans. Autom. Control*, vol. 56, no. 10, pp. 2456–2461, Oct. 2011.
[22] R. Postoyan, P. Tabuada, D. Nesic, and A. Anta, "A framework for the event-triggered stabilization of nonlinear systems," *IEEE Trans. Autom. Control*, vol. 60, no. 4, pp. 982–996, Apr. 2015.
[23] X.-H. Chang, R. Huang, and J. H. Park, "Robust guaranteed cost control under digital communication channels," *IEEE Trans Ind. Informat.*, vol. 16, no. 1, pp. 319–327, Jan. 2020.
[24] X.-H. Chang, R. Huang, H. Wang, and L. Liu, "Robust design strategy of quantized feedback control," *IEEE Trans. Circuits Syst. II, Exp. Briefs*, to be published, doi: 10.1109/TCSII.2019.2922311.
[25] D. Liu and G.-H. Yang, "Neural network-based event-triggered MFAC for nonlinear discrete-time processes," *Neurocomputing*, vol. 272, pp. 356–364, Jan. 2018.
[26] A. Sahoo and S. Jagannathan, "Stochastic optimal regulation of nonlinear networked control systems by using event-driven adaptive dynamic programming," *IEEE Trans. Cybern.*, vol. 47, no. 2, pp. 425–438, Feb. 2017.
[27] A. Sahoo, H. Xu, and S. Jagannathan, "Approximate optimal control of affine nonlinear continuous-time systems using event-sampled neurodynamic programming," *IEEE Trans. Neural Netw. Learn. Syst.*, vol. 28, no. 3, pp. 639–652, Mar. 2017.
[28] J. F. Guerrero-Castellanos, J. J. Téllez-Guzmán, S. Durand, N. Marchand, J. U. Alvarez-Muñoz, and V. R. González-Díaz, "Attitude stabilization of a quadrotor by means of event-triggered nonlinear control," *J. Intell. Robotic Syst.*, vol. 73, nos. 1–4, pp. 123–135, Jan. 2014.
[29] R. Postoyan, M. C. Bragagnolo, E. Galbrun, J. Daafouz, D. Nešić, and E. B. Castelan, "Event-triggered tracking control of unicycle mobile robots," *Automatica*, vol. 52, pp. 302–308, Feb. 2015.
[30] B. Xu and P. Zhang, "Composite learning sliding mode control of flexible-link manipulator," *Complexity*, vol. 2017, pp. 1–6, Aug. 2017.
[31] P. G. Thomasson, "Equations of motion of a vehicle in a moving fluid," *J. Aircr.*, vol. 37, no. 4, pp. 630–639, Jul. 2000.
[32] H. K. Khalil, *Nonlinear Systems*. Englewood Cliffs, NJ, USA: Prentice-Hall, 1996.
[33] S. J. Yoo, "Distributed consensus tracking for multiple uncertain nonlinear strict-feedback systems under a directed graph," *IEEE Trans. Neural Netw. Learn. Syst.*, vol. 24, no. 4, pp. 666–672, Apr. 2013.
[34] M. M. Polycarpou, "Stable adaptive neural control scheme for nonlinear systems," *IEEE Trans. Autom. Control*, vol. 41, no. 3, pp. 447–451, Mar. 1996.
[35] P. A. Ioannou and P. V. Kokotovic, *Adaptive Systems With Reduced Models*. New York, NY, USA: Springer-Verlag, 1983.

JIN HOE KIM received the B.S. degree from the School of Electrical and Electronics Engineering, Chung-Ang University, Seoul, South Korea, in 2019, where he is currently pursuing the master's degree with the Department of Electrical and Electronic Engineering. His current research interests include nonlinear adaptive control, intelligent control using neural networks, and their applications to flight systems.

SUNG JIN YOO received the B.S., M.S., and Ph.D. degrees in electrical and electronic engineering from Yonsei University, Seoul, South Korea, in 2003, 2005, and 2009, respectively. He was a Postdoctoral Researcher with the Department of Mechanical Science and Engineering, University of Illinois at Urbana–Champaign, Champaign, IL, USA, from 2009 to 2010. Since 2011, he has been with the School of Electrical and Electronics Engineering, Chung-Ang University, Seoul, where he is currently a Professor. His research interests include nonlinear adaptive control, decentralized control, distributed control, fault-tolerant control, and neural networks theories, and their applications to robotic, flight, nonlinear time-delay systems, large-scale systems, and multiagent systems.